

# Angular Distributions of Molecular Photofragments by Intense Ultrashort Laser Pulses

Received Aug. 19, 2018,  
Accepted Oct. 15, 2018,

Kai-Jun Yuan<sup>a</sup> and Chuan-Cun Shu<sup>b,\*</sup>

DOI: 10.4208/jams.081918.101518a

<http://www.global-sci.org/jams/>

**Abstract.** We theoretically study the photofragmentation reaction of the hydrogen molecular ion  $H_2^+$  by a single intense ultrashort laser pulse. Simulation results obtained from numerical solutions of time-dependent Schrödinger equations show that quantum interference patterns are constructed in the photofragment spectra and the induced angular distributions of photofragments are sensitive to the wavelength of the laser pulse. These phenomena are successfully explained by using the concept of the light-induced conical intersection.

## 1. Introduction

Imaging and manipulating chemical reactions of molecules by ultrafast laser pulses has been a longstanding goal of photochemistry and photobiology sciences [1-4]. The pump-probe technique by projecting the initial state onto accessible electronic excited states associated with nuclear motion in the femtosecond ( $1\text{fs}=10^{-15}\text{ s}$ ) time regime has been developed as an efficient spectroscopy tool [5]. One thus can obtain detailed and substantiated views on the nuclear dynamics in a molecular system, i.e., the dynamics of intramolecular processes and time evolution of the molecular reaction configurations. The essence is to create a coherent wave packet in the molecular system, thus allowing to control quantum coherence and interference phenomena typically by shaping temporal electromagnetic fields. Recent developments of ultrafast laser pulses provide new tools necessary for investigating electron dynamics on its natural attosecond ( $1\text{as}=10^{-18}\text{ s}$ ) time scale as compared to the slower nuclear motion on the femtosecond time scale [6,7]. One can now separately study the dynamics of electrons and nuclei and observe pure electronic quantum effects without interference from nuclear motion [8, 9]. Attosecond pulses can induce charge migration across a molecular structure [10, 11], leading to quantum control of chemical reactions on the electron nature time scale [12, 13].

The evolution of the vibration-rotational wave packets in which several vibrational states undergo simultaneously coherent excitation illustrates the intramolecular dynamics of nuclei. Ultrashort laser pulses have provided an access to the coherent excitation of molecular vibrations/rotations. It has been theoretically predicted that the phenomena of the single-pulse-induced quantum interference can be observed in the modulation of angular photodissociation products, providing a direct signature of light-induced conical intersection (LICI) in diatomic molecules [14-16]. Such phenomena have been observed in recent experiments by a transform-limited 30 fs

pulse at 795 nm with a peak intensity of  $2\times 10^{13}\text{ W/cm}^2$  into  $H_2^+$  [17]. Most recently, it has been shown that the molecular property of laser-induced quasibound states can be extracted from the transient photofragment momentum distributions, offering a feasible approach to gain an insight into the reaction intermediate directly from photochemical reaction products [18]. These ultrafast phenomena can be understood and analyzed in the framework of light-induced potential (LIP) [1,19-23], which has been commonly used to understand many strong field induced phenomena, including bond softening [24], bond hardening [25], above threshold dissociation (ATD) [26-28], dynamical quenching [29], and stimulated Raman adiabatic passage [30-33].

In the present work we study the molecular photodissociation by a single intense ultrashort laser pulse. Results are obtained from numerical solutions of the time-dependent Schrödinger equation (TDSE) for the benchmark molecular system  $H_2^+$  which has been completely investigated both theoretically and experimentally [34]. It is found that the photofragment angular distributions of molecules are strongly sensitive to the frequency (wavelength) of the driving pulse. Quantum interference patterns are produced at the higher frequency regime. We describe these phenomena by using the

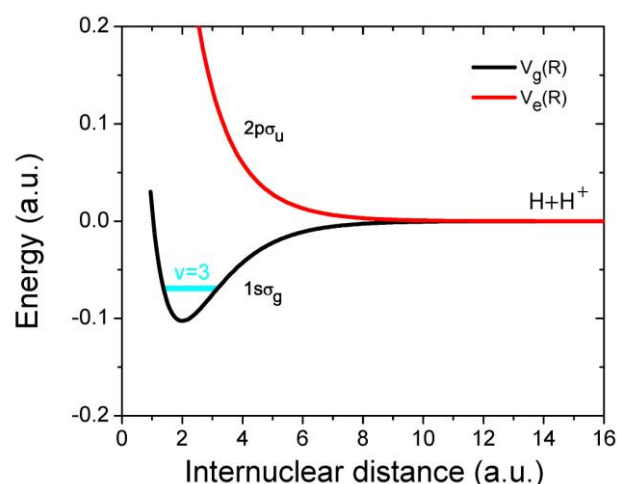


**Figure 1:** Potential energy curves of  $H_2^+$  as a function of internuclear distance  $R$ . The field-free energies of (black line) the ground  $1s\sigma_g$  state and (red line) the rst excited  $2p\sigma_u$  state.  $v=3$  is the initial vibrational level in the ground  $1s\sigma_g$  state.

<sup>a</sup> Institute of Atomic and Molecular Physics, Jilin University, Changchun, 130012, China

<sup>b</sup> Basic Institute of Super-microstructure and Ultrafast Process in Advanced Materials, School of Physics and Electronics, Central South University, Changsha 410083, China

Corresponding author: Email: cc.shu@csu.edu.cn

concepts of LIPs and the LICl in the adiabatic Floquet representation. Throughout this paper, atomic units (a.u.) are used unless otherwise stated.

## 2. Numerical Methods

As schematically illustrated in **Figure 1**, the diatomic molecular ion  $\text{H}_2^+$  interacts with an intense ultrashort laser pulse  $E(t)$ . The potential energy surfaces for the two electronic states, the  $1s\sigma_g$  and the  $2p\sigma_u$  states, are taken from Refs. [35,36]. The time evolution of the wave function  $\psi(t)$  of molecular ions  $\text{H}_2^+$  is computed by solving numerically the TDSE,

$$i \frac{\partial}{\partial t} = H(t)\psi(t) \quad (1)$$

where  $H = H_0 + H_L$  is the total Hamiltonian with

$$H_0 = -\frac{1}{2m} \frac{\partial^2}{\partial^2 R} - \frac{1}{2mR^2} \frac{1}{\sin\theta} \frac{\partial}{\partial\theta} \left( \sin\theta \frac{\partial}{\partial\theta} \right) - \frac{1}{2mR^2 \sin^2\theta} \frac{\partial^2}{\partial^2\phi} + \begin{bmatrix} V_g(R) & 0 \\ 0 & V_e(R) \end{bmatrix} \quad (2)$$

where  $m$  is the reduced mass of the molecule  $\text{H}_2^+$ , and  $R$ ,  $\theta$  and  $\phi$  denote the spherical coordinates of the internuclear vector  $\mathbf{R}$  in the laboratory frame.  $V_g(R)$  and  $V_e(R)$  are the potential energy curves of the  $1s\sigma_g$  and  $2p\sigma_u$  states, as shown in **Figure 1**. In the present work, a linearly polarized laser field is used to dissociate the molecular ion  $\text{H}_2^+$ . Due to the cylindrical symmetry of  $H_0$ , the motion associated with the azimuthal angle can be separated and  $M$  is a good quantum number ( $\Delta M = 0$ ). The field-molecule interaction term  $H_L$  reads as

$$H_L(R, \theta, t) = -\mu(R)\cos\theta E(t), \quad (3)$$

where  $\mu$  is the transition dipole momentum and  $E(t) = E_0 f(t)\cos\omega t$  is the driving laser field with a Gaussian envelope  $f(t) = \exp[-4\ln 2(t/\tau)^2]$ .  $E_0$  is the field amplitude corresponding to maximum intensity  $I_0 = c\varepsilon_0 E_0^2/2$  and  $\tau$  denotes the full width at half maximum (FWHM) of the laser pulse.

The TDSE in Equation (1) is solved numerically by using the split operator method combined with the discrete variable representation (DVR) technique [37, 38]. To avoid reflection of the dissociating wave packet from the end of the grid, an absorption potential  $G(R)$  is added at the boundary of the grid. The energy-dependent distribution of the fragments resulting from the ATD can be obtained by calculating the outgoing flux in momentum space [41, 42]. At an asymptotic point  $R_0$  along the internuclear axis, where the field-molecule interaction is negligible and the absorption potential  $G(R)$  is not switched on, the angle- and time-dependent flux can be expressed as

$$\mathcal{F}(\theta, t)|_{R_0} = \Re \left[ -\frac{i}{m} \psi^*(R_0, \theta, t) \frac{\partial \psi(R, \theta, t)}{\partial R} \Big|_{R_0} \right] \quad (4)$$

The discrete Fourier expansion of  $\psi(R_0, \theta, t)$  is given by

$$\psi^*(R_0, \theta, t) = \frac{1}{N} \sum_{n=1}^N \tilde{\psi}(k_n, \theta, t) e^{2i\pi(n-1)(n_0-1)} \quad (5)$$

where wave vector  $k_n = (2n\pi)/(R_{max} - R_{min})$ , and  $\tilde{\psi}(k_n, \theta, t)$  is evaluated by a discrete Fourier transform  $\psi(k_n, \theta, t)$ . Combining Eqs. (4) and (5) one then obtains,

$$\mathcal{F}(k_n, \theta, t)|_{R_0} = \Re \{ \psi^*(R_0, \theta, t) e^{2i\pi(n-1)(n_0-1)/N} \times \frac{2\pi(n-1)}{m(R_{max}-R_{min})} \tilde{\psi}(k_n, \theta, t), \quad (6)$$

where  $R_{max}$  and  $R_{min}$  are the maximum and minimum grid range.  $\mathcal{F}(k_n, \theta, t)|_{R_0}$  for  $n \in [1, N/2]$  corresponds to the outgoing flux and the other components is negligible [41,42].

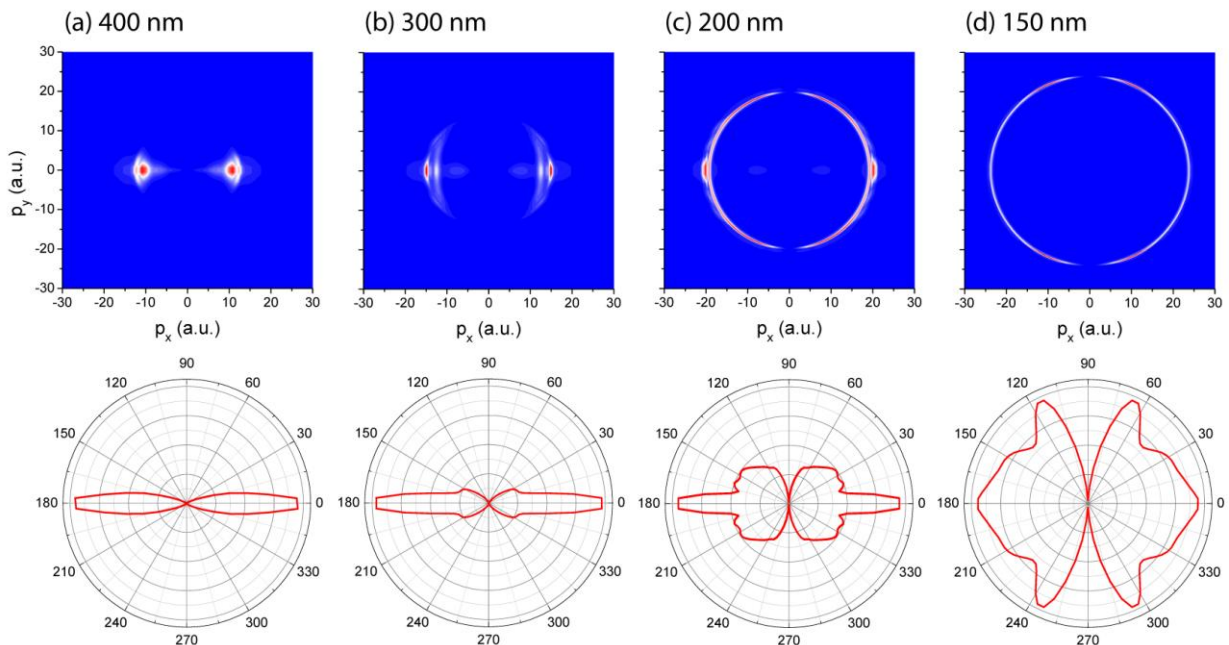


**Figure 2:** Photofragment momentum and angular distributions of  $\text{H}_2^+$  by intense ultrashort laser pulses at wavelengths (a)  $\lambda = 400$  nm ( $\omega = 0.144$  a.u.), (b) 300 nm (0.152 a.u.), (c) 200 nm (0.228 a.u.), and (d) 150 nm (0.304 a.u.). The pulse intensity  $I_0 = 10^{14}$  W/cm<sup>2</sup> ( $E_0 = 5.34 \times 10^{-2}$  a.u.) and duration 20 fs FWHM are always fixed. The signal intensities are arbitrary units.

The energy- and angle- resolved distributions of the photofragments can be expressed as

$$\mathcal{F}(E_n, \theta) = \int dt \mathcal{F}(K_n, \theta, t). \quad (7)$$

$E_n = k_n^2/2m$  is the energy of the photodissociated fragments.

### 3. Results and Discussions

**Figure 2** displays molecular photofragments of  $\text{H}_2^+$  calculated by Eq. (7) by intense ultrashort pulses at different wavelengths. The initial wave function of the molecule is prepared on the 4th vibrational level  $v=3$  of the ground  $1s\sigma_g$  state. The angular quantum and magnetic numbers are always set as  $J=0$  and  $M=0$ . The center wavelength of the pulse varies from  $\lambda=400$  nm ( $\omega=0.114$  a.u.) to 150 nm (0.304 a.u.). The pulse duration at FWHM and intensity are, respectively,  $\tau=20$  fs and  $I_0=10^{14}$  W/cm<sup>2</sup>.

From **Figure 2(a)** we see that the photofragment angular distributions are sensitive to the pulse wavelength  $\lambda$

(frequency  $\omega$ ). At  $\lambda=400$  nm, photofragments are mainly localized at momentum  $p=13.0$  a.u., corresponding to  $p=\sqrt{2m(\omega-E_{v=3})}$ . In **Figure 2(a)**, after absorption of one  $\omega=0.14$  a.u. photon, the molecule is dissociate to  $\text{H}_2^+ \rightarrow \text{H} + \text{H}^+$ . The photodissociation angular distributions are mainly along the laser polarization direction and exhibit symmetry structure in the forward ( $p_x > 0$  or  $\theta = 0$ ) and backward ( $p_x < 0$  or  $\theta = 180^\circ$ ) directions. Increasing the wavelength  $\lambda$  and decreasing the frequency  $\omega$  of the pulses leads to a distortion of the photofragment angular distributions. Multiple angular nodes are obtained in the photofragments. It is also found that at  $\lambda=200$  nm, angular nodes around angles  $n\pi$  and  $\theta = n\pi \pm \pi/6$ , where  $n=0, \pm 1, \pm 2, \dots$ , occur. As the wavelength increases further, angular distributions display more angular nodes. At  $\lambda=150$  nm, the maxima of the angular distributions appear at angles  $\theta = n\pi, n\pi \pm \pi/6, n\pi \pm 3\pi/8$ . As we discussed next, the angular nodes of the photofragment angular distributions arise from the interference effect between the molecular rotational coherent wavepackets during dissociation processes, which depend on the pulse wavelength  $\lambda$ .

To understand these dynamical processes in **Figure 2**, we adopt the concept of LIP in the adiabatic representation [43, 44]. In the adiabatic representation, the two time-dependent LIPs  $V_g^{\text{LIP}}(R, \theta, t)$  and  $V_e^{\text{LIP}}(R, \theta, t)$ , by diagonalizing the  $2 \times 2$  potential matrix of Eq. (2) in rotating wave approximation frame, read as

$$V_g^{\text{LIP}}(R, \theta, t) = \frac{1}{2} [V_e(R) - \omega + V_g(R)] - \sqrt{\Delta^2 + 4C^2(t)}, \quad (8)$$

and

$$V_e^{\text{LIP}}(R, \theta, t) = \frac{1}{2} [V_e(R) - \omega + V_g(R)] + \sqrt{\Delta^2 + 4C^2(t)}, \quad (9)$$

where the detuning  $\Delta = V_e(R) - \omega - V_g(R)$ , and the nonadiabatic coupling term  $C(t) = -\frac{1}{2}\mu(R)\varepsilon_0 f(t)\cos\theta$ . The two LIPs are degenerate at  $\Delta=0$  and  $C(t)=0$ . The LICl is produced in the molecule  $\text{H}_2^+$ , and its position is determined by the carrier frequency  $\omega$ . For comparison, we consider the two cases at  $\lambda=400$  nm and 200 nm in **Figure 2(a)** and **2(c)**. **Figure 3** shows these corresponding LIPs  $V_g^{\text{LIP}}(R, \theta, t)$  and  $V_e^{\text{LIP}}(R, \theta, t)$  by the laser pulses at (a)  $\omega=400$  nm and (b) 200 nm. The maxima of the gap between the two LIPs occur at the angles  $\theta=0$  and  $\pi$ , whereas at the angle of  $\theta=\pi/2$  the LICIs are created at the internuclear distances  $R_{\text{Cl}} \approx 3.85$  a.u. and 2.89 a.u.

We initially prepare the molecular system in the rovibrational level ( $v=3; J=M=0$ ) of the ground electronic state with an eigenenergy  $E_{vJM} = -0.068$  a.u.. At  $\lambda=200$ nm, the LICl energy point is lower than the energy of the  $vJM=3,0,0$  level. The adiabatic wave packet in the upper LIP,  $V_e^{\text{LIP}}$  is trapped temporarily, resulting in chemical bond hardening, and is further rotated to the direction of  $\theta=\pi/2$ . During the dissociation process by the  $\lambda=200$ nm pulse, the excited wavepackets evolve simultaneously on both the lower LIP  $V_g^{\text{LIP}}$  and the upper LIP  $V_e^{\text{LIP}}$ . Due to the LICl that is created around  $\theta=\pi/2$ , a part of adiabatic wave packet moves to the lower LIP,  $V_g^{\text{LIP}}$ . As a result, the interference between the part of the wave packets on the adiabatic LIP  $V_g^{\text{LIP}}$  and the portion of non-adiabatic population transition from  $V_e^{\text{LIP}}$  occurs, giving rise to angular nodes in distributions of photofragments in **Figure 2(c)**. However for the case by the lower frequency (longer wavelength) pulse, the energy are below the LICl. As shown in **Figure 3(a)**, the  $\lambda=400$ nm pulse leads to a bond-

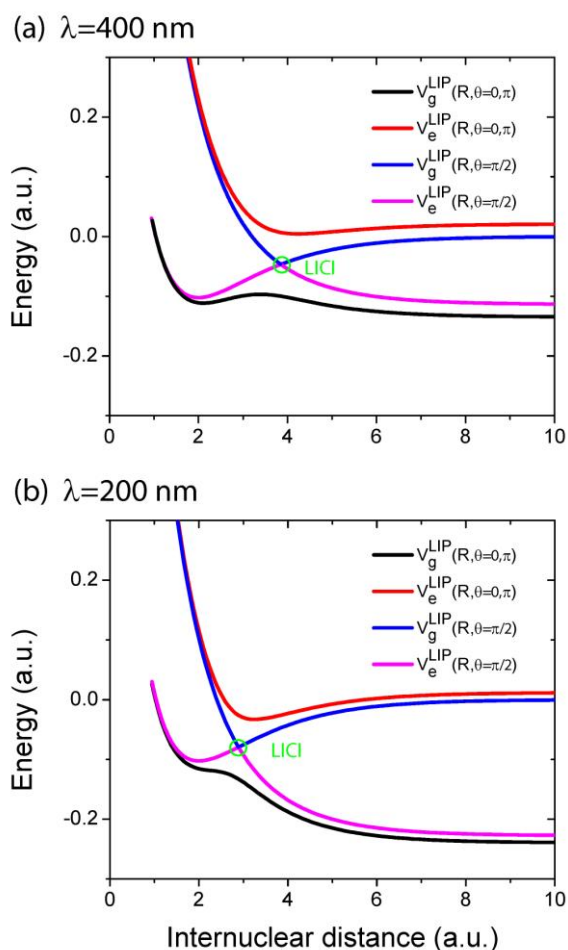


**Figure 3:** Adiabatic Floquet potential curves as a function of molecular internuclear distance  $R$  at different angles  $\theta=0$  and  $\pi/2$ , where  $\theta$  is the angle between the laser polarization and the molecular  $R$  axis, by  $I_0=10^{14}$  W/cm<sup>2</sup> laser fields at wavelengths (b)  $\lambda=400$ nm and (c)  $\lambda=200$ nm. The corresponding lightinduced conical intersections (LICl) are induced respectively at  $R=3.85$  a.u. and 2.89 a.u. for  $\pi/2$ .

soften process. Therefore, no interference occurs, thus resulting in angle distributions along the laser polarization direction, as illustrated in **Figure 2(a)**.

We next display the evolution of the adiabatic wave packets  $\psi_{g/e}^{LIP}(t)$  with time. **Figure 4** shows the time-dependent angular probability distributions  $\mathcal{P}_{g/e}^{LIP}(\theta, t)$  of the adiabatic wave packet probability density obtained by integrating the radial degree  $R$ . The density probability distributions associated with the adiabatic Floquet channels are given by

$$\mathcal{P}_{g/e}^{LIP}(\theta, t) = \left| \int dR \psi_{g/e}^{LIP}(R, \theta, t) \right|^2 \quad (10)$$

where the corresponding adiabatic wave functions  $\psi_{g/e}^{LIP}(R, \theta, t)$  are obtained by [1]

$$\begin{bmatrix} \psi_g^{LIP}(R, \theta, t) \\ \psi_e^{LIP}(R, \theta, t) \end{bmatrix} = \begin{bmatrix} \cos[\eta(R, \theta, t)] & \sin[\eta(R, \theta, t)] \\ -\sin[\eta(R, \theta, t)] & \cos[\eta(R, \theta, t)] \end{bmatrix} \begin{bmatrix} \psi_g(R, \theta, t) \\ \psi_e(R, \theta, t) \end{bmatrix} \quad (11)$$

The rotation angle  $\eta(R, \theta, t)$  (in the two electronic state space) giving rise to the transformation of the diabatic ground electronic  $1s_g$  and the excited  $2p\sigma_u$  states onto the Floquet adiabatic channels is given by

$$\eta(R, \theta, t) = \frac{1}{2} \tan^{-1} \left[ \frac{2\mu(R)E(t)\cos\theta}{V_g(R) - V_e(R) - \omega} \right]. \quad (12)$$

**Figure 4** shows different evolution processes of the adiabatic wave packets. The upper and lower adiabatic potentials,  $V_e^{LIP}$  and  $V_g^{LIP}$ , are shown to be strongly sensitive to the pulse wavelength  $\lambda$ . For the process by the  $\lambda = 200$  nm

pulse, we plot in **Figure 4(b)** the time-dependent angular probability distributions of the adiabatic wave packets  $\psi_g^{LIP}$  and  $\psi_e^{LIP}$  in the lower adiabatic  $V_g^{LIP}$  and upper  $V_e^{LIP}$  potentials in **Figure 3(b)**. It is found that in the upper adiabatic LIP, the adiabatic wave packets move to the  $\theta = \pi/2$  direction due to the resulting effects of the molecular potential and the laser field, as shown in **Figure 4(b)**. Meanwhile, these adiabatic wave packets  $\psi_e^{LIP}$  transfer non-adiabatically to the lower adiabatic LIP  $V_g^{LIP}$  around  $\theta = \pi/2$  by the LICI. The interference is therefore induced in the LICI region. At the end of the pulse excitation ( $t > 10$  fs), the distributions of the adiabatic wave packets  $\psi_g^{LIP}$  and  $\psi_e^{LIP}$  corresponding to the diabatic  $1s_g$  and  $2p\sigma_u$  electronic states exhibit angle  $\theta$  dependent structures. As a result, interference patterns in the photofragment distributions are obtained in **Figure 2(c)**. Similar dynamical processes occur in the case of  $\lambda = 150$  nm. For those cases by longer wavelength pulses where the initial energy level lower than the LICI, the suppression of the barrier leads to the so-called bond softening. As shown in **Figure 3(a)**, for the dissociation case by the  $\lambda = 400$  nm pulse, in the gap region the transition probability is very large. The interference effect therefore is reduced. The molecule is mainly dissociated around the angles of  $\theta = 0$  and  $\pi$ , as illustrated in **Figure 4(a)**. Consequently, in **Figure 2(a)** the well localized photofragment angular distributions are produced.

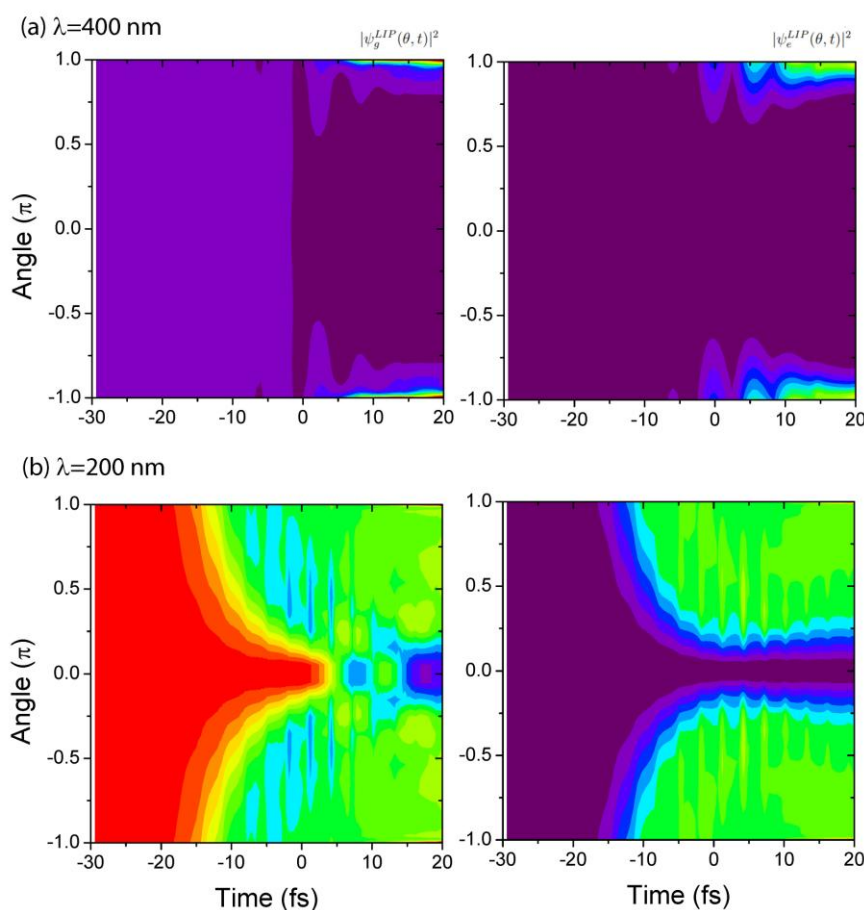


**Figure 4:** Evolutions of angular probability distributions  $\mathcal{P}_{g/e}^{LIP}(\theta, t) = |\psi_{g/e}^{LIP}(\theta, t)|^2$  in Equation (9) with time for (left column) the adiabatic wave packets  $\psi_{g/e}^{LIP}(\theta, t)$ , in the lower adiabatic  $V_g^{LIP}(\theta, t)$  potential and (right column)  $\psi_e^{LIP}(\theta, t)$  in the upper  $V_e^{LIP}(\theta, t)$  potential. The initial wave functions are prepared in the vibrational and rotational ground state (3,0,0). The pulse wavelengths are (a)  $\lambda = 400$  nm and (b) 200 nm, c.f., Fig. 3. The units of the wave packet probability density distributions are arbitrary.

## 4. Conclusions

In summary, we have studied theoretically the photofragment angular distribution in photodissociation of diatomic molecules  $H_2^+$  by an intense ultrashort laser pulse. Simulations are obtained from numerical solutions of TDSEs. Our results have shown that the angular distributions of photofragments exhibit a strong dependence on the wavelength of the driving pulse. At shorter pulse wavelengths, the quantum interference phenomenon has been observed in photofragment angular distributions, whereas for longer wavelength processes the localized distributions along the laser polarization direction are produced. The concept of LIP combined with LICI is adopted for understanding such novel phenomena. The effect of LICI leads to interference effects, thus providing a potential approach to image molecular structures and control molecular reactions.

## Acknowledgements

C.C.S. acknowledges financial support from the National Natural Science Foundation of China (NSFC) under Grant No. 61803389.

## References

- [1] A. D. Bandrauk, *Molecules in Laser Fields* (Marcel Dekker, New York, 1994).
- [2] J. Manz and L. W. Ooste, *Femtosecond Chemistry* (Weinheim: VCH; 1995)
- [3] S. A. Rice and M. Zhao, *Optical Control of Molecular Dynamics* (Wiley, New York, 2000).
- [4] P. W. Brumer and M. Shapiro, *Principle of the Quantum Control of Molecular Processes* (Wiley-Interscience Hoboken, New York, 2003).
- [5] A. H. Zewail, *J. Phys. Chem. A* 104, 5660 (2000).
- [6] F. Krausz and M. Ivanov, *Rev. Mod. Phys.* 81, 163 (2009).
- [7] A. R. Beck, D. M. Neumark, and S. R. Leone, *Chem. Phys. Lett.* 62, 119 (2015).
- [8] A. D. Bandrauk, S. Chelkowski, D. J. Diestler, J. Manz, and K.-J. Yuan, *Int. J. Mass Spectrom.* 277,189 (2008).
- [9] M. Vrakking, *Phys. Chem. Chem. Phys.* 16, 2775 (2014).
- [10] P. M. Kraus, B. Mignolet, D. Baykusheva, A. Rupenyan, L. Horny, E. F. Penka, G. Grassi, O. I. Tolstikhin, J. Schneider, F. Jensen, L. B. Madsen, A. D. Bandrauk, F. Remacle, and H.J. W orner, *Science* 350, 790 (2015).
- [11] G. Hermann, C. Liu, J. Manz, B. Paulus, J. F. Perez-Torres, V. Pohl, and J. C. Tremblay, *J. Phys. Chem. A* 120, 5360 (2016).
- [12] F. Lepine, M. Y. Ivanov, and M. J. J. Vrakking, *Nature Photonics* 8, 195 (2014).
- [13] P. Ranitovic, C. W. Hogle, P. Riviere, A. Palacios, X. M. Tong, N. Toshima, A. Gonzalez-Castrillo, L. Martin, F. Martn, M. M. Murnane, and H. Kaptey, *Proc. Natl Acad. Sci. USA* 111, 912 (2013).
- [14] G. J. Halasz, A. Vibok, H. D. Meyer, and L. S. Cederbaum, *J. Phys. Chem. A* 117, 8528 (2012).
- [15] G. J. Halasz, A. Vibok, and L. S. Cederbaum, *J. Phys. Chem. Lett.* 6, 348 (2015).
- [16] C. C. Shu, D. Dong, and K.-J. Yuan, *Mol. Phys.* 115, 1908 (2017).
- [17] A. Natan, M. R. Ware, V. S. Prabhudesai, U. Lev, B. D. Bruner, O. Heber, and P.H. Bucksbaum, *Phys. Rev. Lett.* 116, 143004 (2016).
- [18] C. C. Shu, K. J. Yuan, D. Dong, I. R. Petersen, and A. D. Bandrauk, *J. Phys. Chem. Lett.* 8, 1 (2017).
- [19] A. D. Bandrauk and M. L. Sink, *Mol. Phys.* 19, 95 (1970).
- [20] A. D. Bandrauk and M. L. Sink, *Chem. Phys. Lett.* 57, 569 (1978).
- [21] A. D. Bandrauk and M. L. Sink, *J. Chem. Phys.* 68, 3040 (1978).
- [22] A. D. Bandrauk and M. L. Sink, *J. Chem. Phys.* 74, 1110 (1981).
- [23] E. E. Aubanel and A. D. Bandrauk, *J. Chem. Phys.* 97, 12620 (1993).
- [24] P. H. Bucksbaum, A. Zavriyev, and H. G. Muller, *Phys. Rev. Lett.* 64, 1883 (1990).
- [25] L. J. Frasinski, J. H. Posthumus, J. Plumridge, K. Codling, P. F. Taday, and A. J. Langley, *Phys. Rev. Lett.* 83, 3625 (1999).
- [26] A. Giusti-Suzor, X. He, O. Atabek, and F. H. Mies, *Phys. Rev. Lett.* 64, 515 (1993).
- [27] P. A. Orr, I. D. Williams, J. B. Greenwood, I. C. E. Turcu, W. A. Bryan, J. Pedregosa-Gutierrez, and C. W. Walter, *Phys. Rev. Lett.* 98, 163001 (2007).
- [28] W. Gao, B. B. Wang, X. J. Hu, S. Chai, Y. C. Han, J.B. Greenwood, *Phys. Rev. A* 96, 013426 (2017).
- [29] H. Abou-Rachid, T. T. Nguyen-Dang, and O. Atabek, *J. Chem. Phys.* 114, 2197 (2001).
- [30] U. Gaubatz, P. Rudecki, S. Schiemann, and K. Bergmann, *J. Chem. Phys.* 92, 5363 (1990).
- [31] B. M. Garraway and K.-A. Suominen *Phys. Rev. Lett.* 80, 932 (1998).
- [32] I. R. Sola, J. Santamarria, and V. S. Malinkovsky, *Phys. Rev. A* 61, 043413 (2000).
- [33] Y. C. Han, *J. Phys. B* 50, 225401 (2017).
- [34] H. Ibrahim, C. Lefebvre, A. D. Bandrauk, A. Staudte, and F. Legare, *J. Phys. B* 51, 042002 (2018).
- [35] F. V. Bunkin and I. I. Tugov, *Phys. Rev. A* 8 601 (1973).
- [36] S. I. Chu, C. Laughlin, and K. Datta, *Chem. Phys. Lett.* 98, 476 (1983).
- [37] Z. Sun, L. Liu, S. Y. Lin, R. Schinke, H. Guo, D. H. Zhang, *Proc. Natl. Acad. Sci. USA* 107, 555 (2010).
- [38] K. J. Yuan, Z. Sun, S. M. Wang, S. L. Cong, *Chem. Phys. Lett.* 414 (1-3), 180 (2005).
- [39] G. Jolicard, G. D. Billing, *Chem. Phys.* 149, 261 (1991).
- [40] G. Jolicard, O. Atabek, *Phys. Rev. A* 46, 5845 (1992).
- [41] R. Numico, A. Keller, and O. Atabek, *Phys. Rev. A* 60, 406 (1999).
- [42] R. Numico, A. Keller, and O. Atabek, *Phys. Rev. A* 52, 1298 (1995).
- [43] S. I. Chu, *J. Chem. Phys.* 75, 2215 (1981).
- [44] T. T. Nguyen-Dang, C. Lefebvre, H. Abou-Rachid, and O. Atabek, *Phys. Rev. A* 71, 023403 (2005).